Deformation effects in ^{185}Au

P. Joshi,* A Kumar, and I. M. Govil
Department of Physics, Panjab University, Chandigarh 160014, India

R. P. Singh, G. Mukherjee, S. Muralithar, and R. K. Bhowmik
Nuclear Science Centre, Post Box 10502, New Delhi 110067, India

U. Garg
Department of Physics, University of Notre Dame, Notre Dame, Indiana 46556, USA
(Received 12 September 2003; published 2 April 2004)

The nucleus ^{185}Au was populated using the reaction ^{159}Tb(^{30}Si,4n)^{185}Au at 140 MeV beam energy. Lifetimes for the $E2$ transitions in $h_{9/2}$ and $i_{13/2}$ bands have been measured using recoil distance method. The reduced transition probabilities $B(E2)$ and transitional quadrupole moments Q_t were extracted using the measured lifetimes. Calculations of quasiparticle Routhians and total Routhian surfaces (TRS) have been performed to investigate the effect of the β- as well as the γ-driving properties of these configurations in this nucleus.

DOI: 10.1103/PhysRevC.69.044304 PACS number(s): 21.10.Tg, 21.10.Ky, 27.70.+q

I. INTRODUCTION

The deformation-driving properties of the high-j intruder configurations built upon $h_{9/2}$ and $i_{13/2}$ orbitals have been an interesting point of investigation in the $Z=73-79$ and $A=170-180$ mass region [1–7]. It is believed that these orbits belonging to the higher-N shells come down rapidly as a function of the quadrupole deformation β and polarize the nuclear shape towards large β values. Because of their large slopes on the β axis, they do not mix with the other j configurations and hence keep their deformation-driving tendency alive. However, it is still possible for them to mix with the other K configurations of the same j orbital as a function of triaxiality (γ). The net deformation-driving tendency would, therefore, depend upon the slope of the energy of these orbitals in the β -γ two-dimensional surface. Light gold nuclei ($A\sim185$) are good candidates for studying these effects since their proton Fermi level lies closer to these two high-j intruder proton configurations, namely $h_{9/2}[541]1/2^-$ and $i_{13/2}[660]1/2^+$. The $h_{9/2}$ configuration in these nuclei has a quasiparticle nature since it lies closer to the Fermi surface when compared with the $i_{13/2}$ configuration which lies above the Fermi surface and is understood to have the shape polarizing tendency. It is, therefore, generally expected that the band built on the $i_{13/2}$ configuration would have a larger quadrupole deformation compared to the band built on the $h_{9/2}$ configuration. Our previous measurements on ^{183}Au nucleus [6] have shown similar deformation-driving effects. In order to have a more systematic investigation of this effect in this mass region, we have performed lifetime measurements in the rotational bands built upon $h_{9/2}$ and $i_{13/2}$ configurations in the ^{185}Au nucleus.

II. EXPERIMENTAL DETAILS AND DATA ANALYSIS

The reaction ^{159}Tb(^{30}Si,4n) was used to populate high spin states in ^{185}Au. A 140 MeV ^{30}Si beam was provided by the 15 UD pelletron accelerator at NSC, New Delhi. The Gamma Detector Array [8] consisting of 12 Compton suppressed HPGe detectors was used for detecting the γ rays, with a 14-element BGO array used as a multiplicity filter.

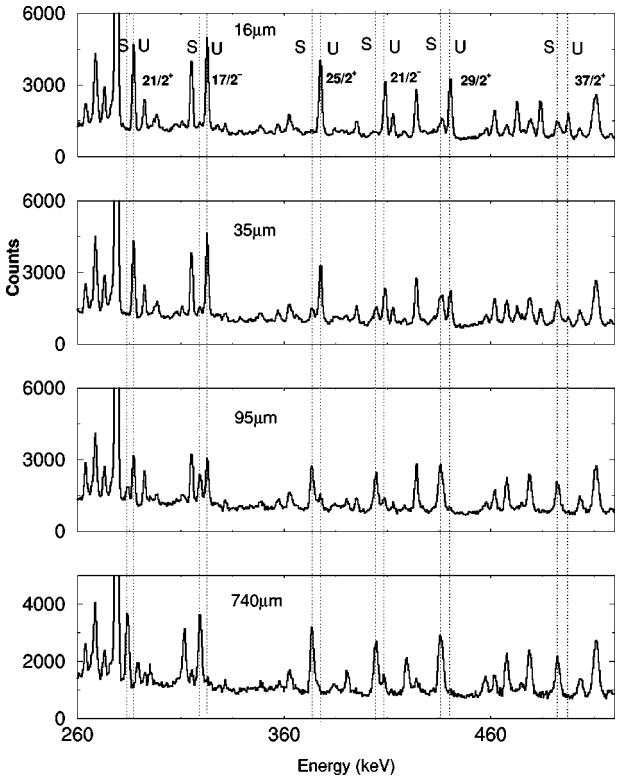

FIG. 1. The shifted (S) and unshifted (U) peaks at various target to stopper distances for ^{185}Au nucleus.

*Present address: Physics Department, University of York, YO10 5DD, York, UK.

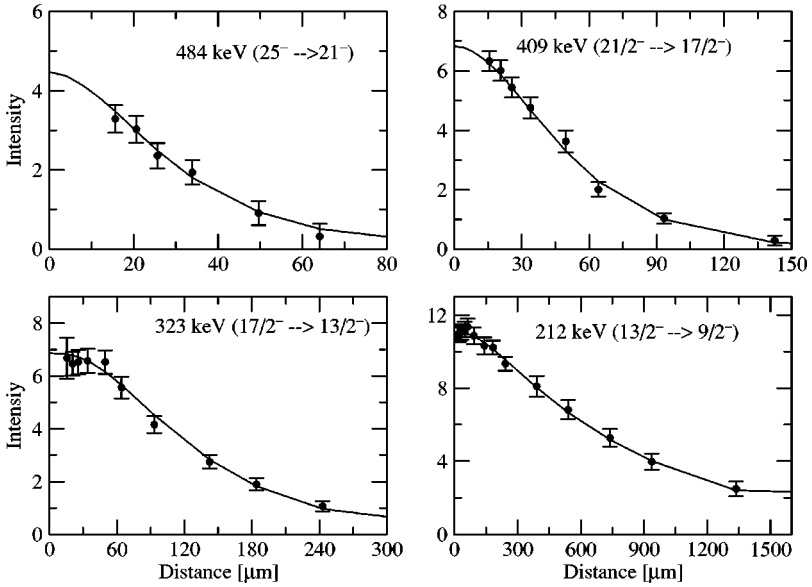

FIG. 2. The decay curves for the transitions of positive parity $i_{13/2}$ band in ^{185}Au nucleus.

The singles data were hardware gated by the condition that at least two or more BGO detectors fired in coincidence with the Compton suppressed germanium signal. The NSC Recoil Distance Device [3] has been used for stopping the fast moving recoils from the target in the stopper. The target consisted of a 1 mg/cm^2 ^{159}Tb thick foil stretched on a finely polished cone. An 8 mg/cm^2 thick gold stopper foil was mounted on a similar cone located downstream facing the target. The distance between the stopper and the target was calibrated using the capacitance method [9] and the minimum distance was found to be 10 μm. The measurements were made for distances starting from 10 μm to 10 000 μm. The data at larger distances were used to take into account the effect of any long lived side-feeding transitions. The velocity of recoiling ^{185}Au nuclei was found to be $v/c=0.0155$, from measured Doppler shifts of known transitions. This value of v/c has been used for the lifetime analysis.

Spectra showing the shifted and the unshifted peaks for various transitions of the $h_{9/2}$ and $i_{13/2}$ bands at different target to stopper distances are shown in Fig. 1. The intensities of the different transitions in the $h_{9/2}$ and $i_{13/2}$ bands as a function of the target to stopper distances are shown in Fig. 2 and 3, respectively. These intensities were fitted to the decay curves using the program LIFETIME [10]. The procedure for fitting was to start from the topmost level observed in the experiment which was being fed from the top by a band of known transitions with an effective quadrupole moment. The fitted intensities and lifetimes for this transition were then used as the starting parameters for the top feeding of the transition immediately below that. The unknown side-feeding intensities have been taken into account during the fitting procedure. The starting values of the side-feeding intensities have been estimated from the intensity balance. This fitting procedure may introduce a systematic error up to 10% in the lifetime measurements. The change in the detector solid angle due to the movement of the target position and the alignment attenuation corrections [10] were also made in the analysis. The error analysis has been done by the com-

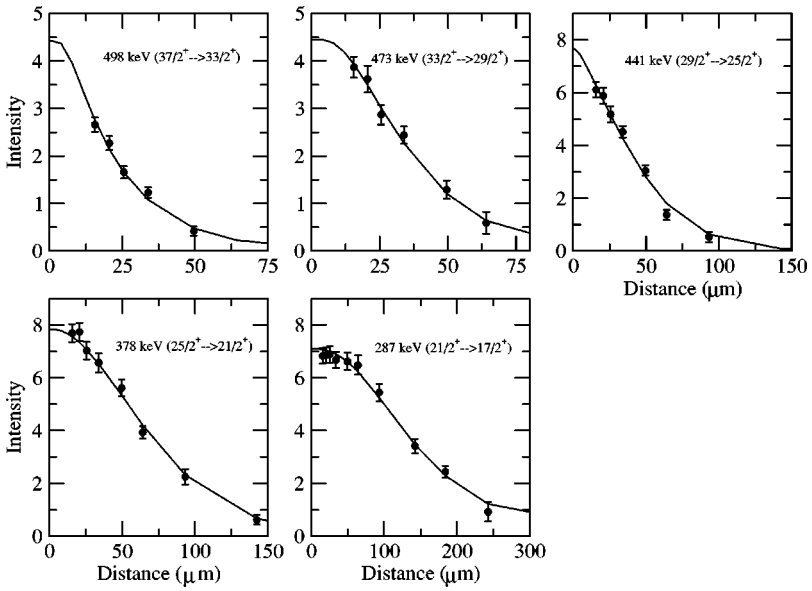

FIG. 3. The decay curves for the transitions of negative parity $h_{9/2}$ band in ^{185}Au nucleus.

TABLE I. Lifetimes and the $B(E2)$ values for the positive parity $i_{13/2}$ band in ^{185}Au.

Energy (keV)	Transition $(I_i^\pi \rightarrow I_f^\pi)$	Lifetime (ps)	$B(E2)$ $(e^2\ b^2)$
287	$\frac{21}{2}^+ \rightarrow \frac{17}{2}^+$	$23.3^{1.8}_{1.8}$	$1.60^{0.13}_{0.11}$
378	$\frac{25}{2}^+ \rightarrow \frac{21}{2}^+$	$6.99^{0.44}_{0.43}$	$1.45^{0.10}_{0.09}$
441	$\frac{29}{2}^+ \rightarrow \frac{25}{2}^+$	$4.00^{0.15}_{0.17}$	$1.19^{0.05}_{0.04}$
473	$\frac{33}{2}^+ \rightarrow \frac{29}{2}^+$	$3.33^{+0.19}_{-0.29}$	$1.00^{0.07}_{0.11}$
498	$\frac{37}{2}^+ \rightarrow \frac{33}{2}^+$	<4.12	>0.63

puter routine MINUIT [11] which calculates the errors as the deviation on both sides of the minimum corresponding to a unit increment in the normalized χ^2 value.

III. RESULT AND DISCUSSION

A. Experimental results

The measured lifetimes were used for calculating the reduced transition probabilities for the transitions. The reduced transition probabilities were calculated using the relation

$$B(E2) = (0.08156)/[E_\gamma^5 \tau(1+\alpha_\tau)]\ e^2\ b^2, \qquad (1)$$

where E_γ is the γ-ray energy in MeV, τ is the lifetime in picosecond, and α_τ is the total electron conversion coefficient. The reduced transition probabilities extracted from the measured lifetimes for the various transitions of the $h_{9/2}$ and $i_{13/2}$ bands are tabulated in Tables I and II, respectively.

In order to have an idea of the shapes associated with the two configurations, these $B(E2)$ values were used for extracting the transition quadrupole moments for these two bands using the relation

$$Q_t = \frac{[16\pi B(E2)]^{1/2}}{\sqrt{5}\langle IK20|I-2K\rangle}. \qquad (2)$$

The extracted quadrupole moments for both the bands are plotted in Fig. 4. It is clear from the figure that the quadrupole moments for the $i_{13/2}$ band transitions are systematically higher than those for the $h_{9/2}$ band. The $i_{13/2}$ band which is built upon the high-j configuration is expected to have more deformation due to the deformation-driving tendency. The $h_{9/2}$ band on the contrary is likely to be less deformed since it lacks the deformation-driving tendency. An interesting observation apparent from Fig. 4 is that the transition quadrupole moments Q_t decrease as a function

TABLE II. Lifetimes and the $B(E2)$ values for the negative parity $h_{9/2}$ band in ^{185}Au.

Energy (keV)	Transition $(I_i^\pi \rightarrow I_f^\pi)$	Lifetime (ps)	$B(E2)$ $(e^2\ b^2)$
212	$\frac{13}{2}^- \rightarrow \frac{9}{2}^-$	168^{16}_{14}	$0.86^{0.05}_{0.05}$
323	$\frac{17}{2}^- \rightarrow \frac{13}{2}^-$	$19.5^{1.4}_{1.2}$	$1.09^{0.07}_{0.07}$
409	$\frac{21}{2}^- \rightarrow \frac{17}{2}^-$	$6.16^{0.50}_{0.54}$	$1.10^{0.11}_{0.08}$
484	$\frac{25}{2}^- \rightarrow \frac{21}{2}^-$	<5.06	>0.59

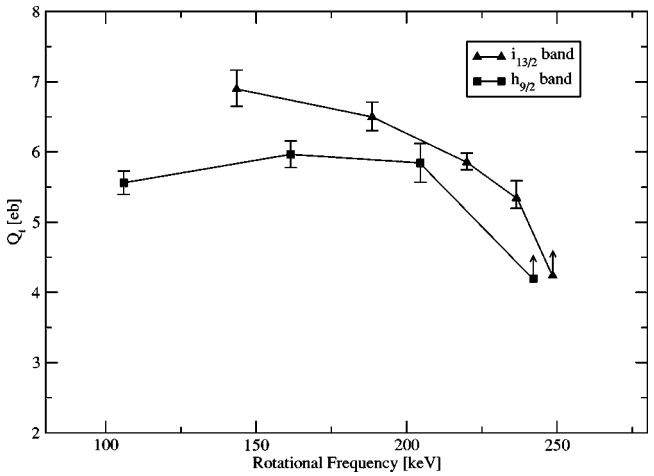

FIG. 4. The transition quadrupole moments extracted from the measured transition probabilities for the $i_{13/2}$ and $h_{9/2}$ bands in ^{185}Au nucleus. The solid lines are the guide to the eye.

of the increasing spin within the band. This trend is visible in both the bands, although it is more pronounced for the $i_{13/2}$ band. The decrease in the Q_t values is likely an indication of a change in shape at higher excitation in the nucleus.

B. Theoretical calculations

In order to investigate the deformation-driving tendencies of the $i_{13/2}$ and the $h_{9/2}$ configurations, we performed theoretical calculations within the framework of cranked shell model. A deformed Woods-Saxon potential parametrized by β, γ, and β_4 has been used in these calculations [12–14]. A monopole pairing interaction [15] has been assumed between the pairs of same type of nucleons. Details of the calculations can be found in Ref. [6] and the references within. Since both β and γ can give rise to changes in the Q_t, it is instruc-

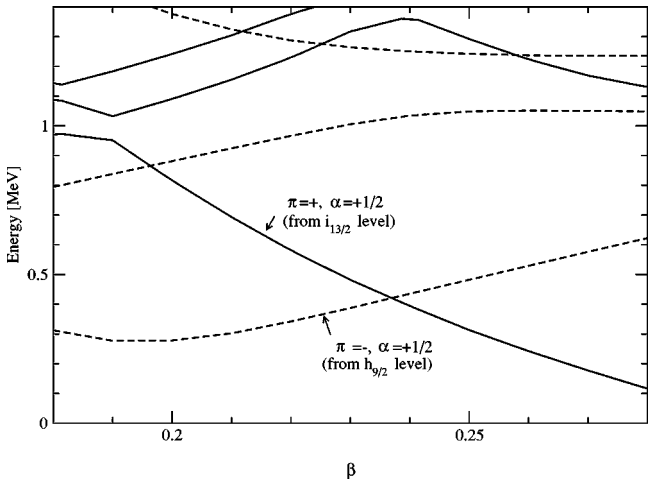

FIG. 5. The quasiproton Routhians for positive parity positive signature (solid line) as well as negative parity positive signature (dashed line), plotted against deformation β at a rotational frequency of $\hbar\omega$=0.25 MeV for ^{185}Au nucleus.

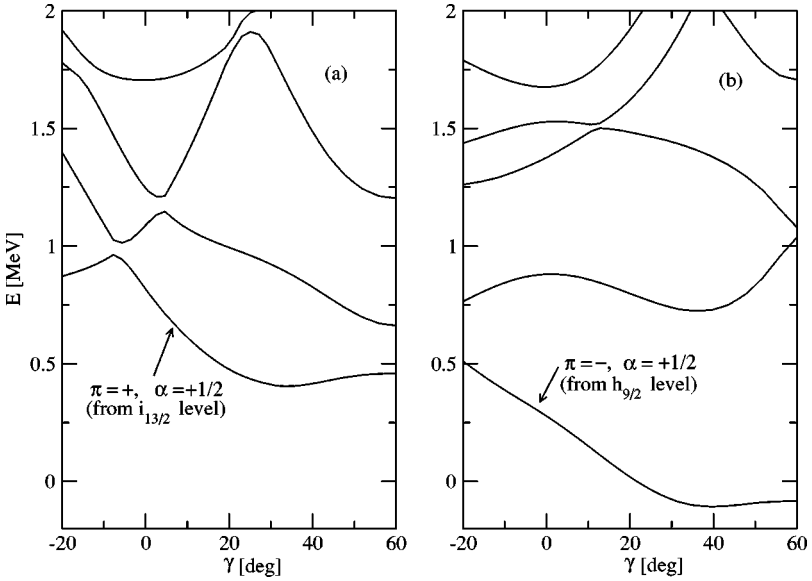

FIG. 6. The quasiproton Routhians for positive parity and positive signature (left), negative parity and positive signature (right), plotted against deformation γ at a deformation $\beta=0.20$ and a rotational frequency of $\hbar\omega=0.25$ MeV for ^{185}Au nucleus.

tive to see the energies of these orbitals as a function of both β as well as γ. Figure 5 shows the quasiparticle energies of the positive parity as well as negative parity states as a function of β for a finite rotation ($\hbar\omega=250$ keV). It is seen from this figure that the level coming from the $i_{13/2}$ configuration goes down in the energy as a function of the quadrupole deformation β. The negative slope of this level for larger β values indicates that it would try to deform the nucleus toward the larger deformation which is in agreement with the experimental observation of the larger average Q_t value for the $i_{13/2}$ band. The slope of the negative parity configuration, on the other hand, is positive as a function of β, thereby indicating that its deformation-driving tendency is opposite and hence expected to be less deformed.

These two different slopes of the quasiparticle configurations arise due to their mixing with their counterpart hole configurations, across the Fermi level, which have opposite slopes to the particle states. The $i_{13/2}$ orbit which has a negative slope has a higher admixture of the particle state compared to the corresponding hole state, hence its overall slope is negative. The situation is opposite for the $h_{9/2}$ level which has more admixture of the hole counterpart and hence it has a net positive slope and, therefore, shows opposite effect. The hole orbitals, available across the Fermi level for mixing with their corresponding particle state, would mix more if the level is close to the Fermi level. Since the level from $h_{9/2}$ configuration is lower than the level from $i_{13/2}$ orbital, its mixing is more with the corresponding hole state while the level from $i_{13/2}$ orbital is still above the proton Fermi level and mixes less with the hole state. This fact influences their respective deformation-driving tendency and hence the $i_{13/2}$ configuration is more prolate deformation driving while the $h_{9/2}$ is slightly oblate driving.

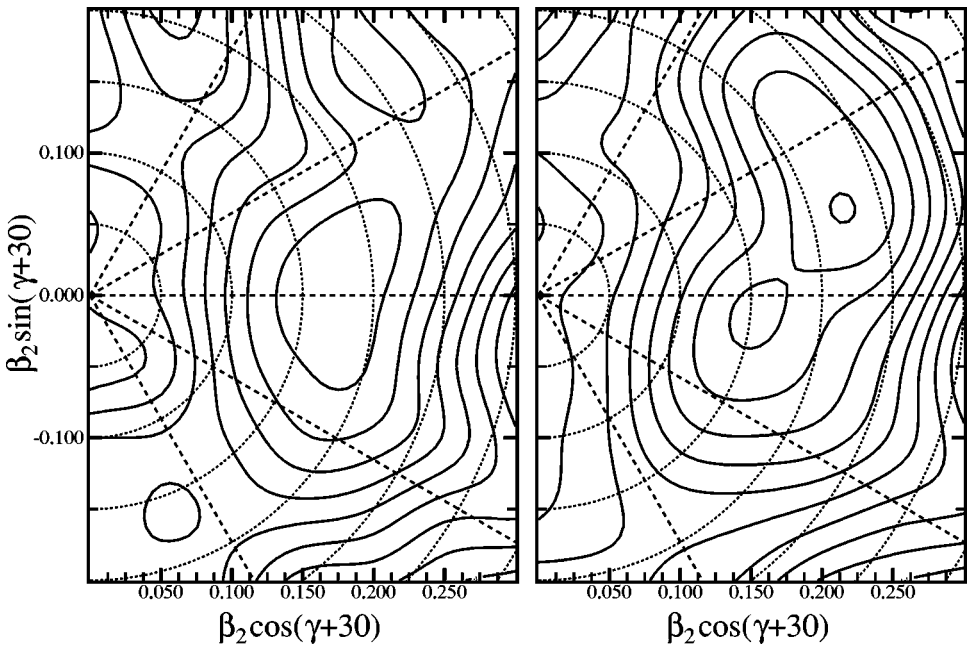

FIG. 7. The TRS plots for the positive parity and positive signature (left) and negative parity and positive signature (right) configurations in ^{185}Au nucleus at a rotational frequency of $\hbar\omega=0.25$ MeV.

In addition to this, a γ-driving tendency of the orbital may also have an impact on the Q_t values. In order to see the γ-driving tendency of these two configurations we calculated the quasiparticle energies as a function of γ. Figures 6(a) and 6(b) show the energies of the positive and negative parity configurations from $i_{13/2}$ and $h_{9/2}$ orbitals as a function of γ at a finite rotation of $\hbar\omega$=250 keV. It is quite clear from these figures that both the $h_{9/2}$ and the $i_{13/2}$ configurations have a tendency for deforming the nucleus toward larger γ values. Since a change towards increasing γ would give rise to the reduction in the quadrupole moment, thus the lowering in the Q_t values at high spins may be an indication of the onset of triaxiality in the nucleus for these configurations. In order to have a look at the shape of the nucleus for these configurations, we performed total Routhian surface (TRS) calculations using the macroscopic-microscopic formalism [13,14,16]. The calculated TRS values in the β-γ plane are shown in Fig. 7 for the positive parity positive signature as well as the negative parity positive signature. It is clear from these plots that there is a strong tendency of the nucleus to attain a triaxial shape for both these configurations. It is, therefore, possible that the decrease in the Q_t values is because of attaining the triaxial shape for both the $h_{9/2}$ as well as $i_{13/2}$ configurations. It is worth mentioning that the large γ softness as seen from these calculations is due to the effect of the added quasiparticle energies to the core.

IV. SUMMARY

We have measured the lifetimes of the $E2$ transitions of the $h_{9/2}$ band and $i_{13/2}$ band using the recoil distance method technique. The measured lifetimes were used for extracting the reduced transition probabilities and the transition quadrupole moments. The extracted Q_t values have been used to understand the nuclear shapes for these two configurations. The data suggest the comparatively large Q_t value of the $i_{13/2}$ band is due to the larger deformation-driving tendency of this configuration as compared to the $h_{9/2}$ configuration. The quasiparticle energies calculated as a function of β also support a larger deformation-driving tendency for this configuration, compared to the $h_{9/2}$ band. The calculations also suggest a large triaxiality caused resulting from the quasiparticle effects. The data also suggest that this γ softness is most likely the reason for the decrease of the Q_t values of these two bands at higher rotational frequencies.

[1] D. Muller *et al.*, Phys. Lett. B **332**, 265 (1994).
[2] W. F. Mueller *et al.*, Phys. Rev. C **59**, 2009 (1999).
[3] P. Joshi *et al.*, Phys. Rev. C **60**, 034311 (1999).
[4] P. Joshi *et al.*, Phys. Rev. C **64**, 034303 (2001).
[5] S. K. Chamoli *et al.*, Phys. Rev. C **66**, 024307 (2002).
[6] P. Joshi *et al.*, Phys. Rev. C **66**, 044306 (2002).
[7] A. J. Larbee *et al.*, Phys. Lett. **169B**, 21 (1986).
[8] S. C. Pancholi and R. K. Bhowmik, Indian J. Pure Appl. Phys. **27**, 660 (1989).
[9] T. K. Alexander and A. Bell, Nucl. Instrum. Methods **81**, 22 (1970).
[10] J. C. Wells *et al.*, ORNL/TM Report No. 9105, 1985.
[11] F. James and M. Roos, Comput. Phys. Commun. **10**, 343 (1975).
[12] W. Nazarewicz, M. A. Riely, and J. D. Garrett, Nucl. Phys. **A512**, 61 (1990).
[13] T. R. Werner and J. Dudek, At. Data Nucl. Data Tables **59**, 1 (1995).
[14] T. R. Werner and J. Dudek, At. Data Nucl. Data Tables **50**, 179 (1992).
[15] S. G. Nilsson and I. Ragnarsson, *Shapes and Shells in Nuclear Structure* (Cambridge University Press, Cambridge, 1995), p. 290.
[16] S. G. Nilsson and I. Ragnarsson, *Shapes and Shells in Nuclear Structure* (Cambridge University Press, Cambridge, 1995), p. 317.